Lab on a Chip

PAPER

View Article Online
View Journal | View Issue

Cite this: *Lab Chip*, 2014, **14**, 1469

Flow metering characterization within an electrical cell counting microfluidic device†

U. Hassan,[ab] N. N. Watkins,‡[ab] C. Edwards§[b] and R. Bashir*[bc]

Received 15th November 2013,
Accepted 24th January 2014

DOI: 10.1039/c3lc51278a

www.rsc.org/loc

Microfluidic devices based on the Coulter principle require a small aperture for cell counting. For applications using such cell counting devices, the volume of the sample also needs to be metered to determine the absolute cell count in a specific volume. Hence, integrated methods to characterize and meter the volume of a fluid are required in these microfluidic devices. Here, we present fluid flow characterization and electrically-based sample metering results of blood through a measurement channelwith a cross-section of 15 μm × 15 μm (*i.e.* the Coulter aperture). Red blood cells in whole blood are lysed and the remaining fluid, consisting of leukocytes, erythrocyte cell lysate and various reagents, is flown at different flow rates through the measurement aperture. The change in impedance across the electrodes embedded in the counting channel shows a linear relationship with the increase in the fluid flow rate. We also show that the fluid volume can be determined by measuring the decrease in pulse width, and increase in number of cells as they pass through the counting channel per unit time.

Introduction

Integrated flow metering is essential in lab-on-a-chip and microfluidic devices. Microfluidic cell counters based on the Coulter counting principle use a small cross-sectional channel or aperture with micro-fabricated electrodes. The impedance across the electrodes increases as a cell passes through the channel and a voltage spike, of which the amplitude is proportional to the cell's size and the width is proportional to the cell's velocity, is produced. The change in impedance also depends on the flow rate at which the fluid is flowing, thus providing an opportunity to meter the fluid volume. Errors in the measurement of a fluid volume can come from the variance in the device channel dimensions, introduction of bubbles, or fluid dead volumes. This could become a significant problem for single blood drop point-of-care devices as only a few microliters of blood is used in these measurements.

Many have shown that flow metering is possible using different sensing mechanisms such as periodic flapping motion detection,[1] thermistor based temperature difference detection with varying flow rates,[2] atomic emission detection using radio RF plasma for nanoscale flow rate metering,[3] rapid scanning using a laser-induced self-mixing effect,[4] and other methods. The heat sensing mechanism works by measuring the temperature difference in a micro channel across two points. However, such sensors are complicated in design as they require heat sensing using (2 reference and 3 sensing) thermistors, and a heat sink to provide insulation on the same device.[2] A microfluidic flow sensor based on a Venturi tube design was shown to meter the volume of deionized water but requires the maintenance of a stable vacuum.[5]

The flow of an electrolyte in a microfluidic channel is given by a parabolic profile when the flow is laminar (Reynolds number < 1) and would result in the redistribution of ions within the electric double layer in the channel.[6–8] When the AC voltage is applied across the channel electrodes, the ions respond to the electrical fields across the electrodes.[9] The electro-kinetic effects result in ionic redistribution, which then results in changing the electrical impedance across the electrodes. Thus, the flow of the fluid in a micro channel can be related to the change in impedance across the micro electrodes.[10–12] The different parameters, including the amplitude of AC voltage, the frequency of the signal, the conductivity of the electrolyte, and the dimensions of the electrodes, need to be optimized for better sensitivity.[6,13] With an increase in flow rate, the mass transport increases due to an increase in the ionic concentration. The mass transport limited current,

[a] *William L. Everett Laboratory, Department of Electrical and Computer Engineering, University of Illinois at Urbana-Champaign, 1406 W. Green St., Urbana, IL 61801, USA*
[b] *Micro and Nanotechnology Lab, University of Illinois at Urbana-Champaign, 208 N. Wright St., Urbana, IL 61801, USA*
[c] *1270 Digital Computer Laboratory, Department of Bioengineering, University of Illinois at Urbana-Champaign, 1304 W. Springfield Ave., Urbana, IL 61801, USA. E-mail: rbashir@illinois.edu*

† Electronic supplementary information (ESI) available. See DOI: 10.1039/c3lc51278a

‡ Present address: Nabsys, Inc., 60 Clifford St., Providence, RI 02903, USA.
§ Present address: Massachusetts Institute of Technology, 77 Massachusetts Ave, Cambridge, MA 02139, USA.

i_L, increases as it is directly proportional to the cube root of the volumetric flow rate, Q, of the fluid, as given by eqn (1) below.[6,14]

$$i_L = 0.925nF\,[A]_{bulk} D_A^{2/3} Q^{1/3} w_e \sqrt[3]{l^2/h^2 w} \quad (1)$$

where, n is the number of electrons transferred, F is the Faraday constant, l is the electrode length, h is the half-height of the cell, w is the width of the cell, w_e is the electrode width and D_A is the diffusion coefficient.[6]

Performing flow metering in a microfluidic device with human blood has many applications in clinical diagnostic devices.[15,16] Recently, we reported a cell counting device for HIV/AIDS diagnostics that takes a drop of blood to count the CD4+ T cells with high accuracy at point-of-care.[17] Using that device design, we show here that we can meter the fluid sample using the same electrodes used to count the cells. In our bio-chip, the whole blood is mixed with a lysing buffer to lyse all erythrocytes and preserve the leukocytes. The remaining fluid, consisting of leukocytes, erythrocyte cell lysate (consisting of the intracellular ions), and the lysing and quenching reagents, is flown at different flow rates through the measurement channel.[17,18] As the erythrocytes get lysed, the release of intracellular ions increases the total ionic concentration in the surrounding fluid. We have characterized the impedance change and cell counts in a fluid *versus* different flow rates and show that these parameters can be used to meter a solution in microfluidic devices.

Experimental setup

The device schematic is shown in Fig. 1a.[17] 10 μL of whole blood is infused in the chip and mixed with lysing reagent (0.12% (v/v) formic acid and 0.05% (w/v) saponin in DI), resulting in the complete lysis of erythrocytes. The resulting solution is then mixed on-chip with a quenching solution (5.3 mL of 0.6% (w/v) sodium carbonate and 3% (w/v) sodium chloride in DI) to halt the lysing process by maintaining

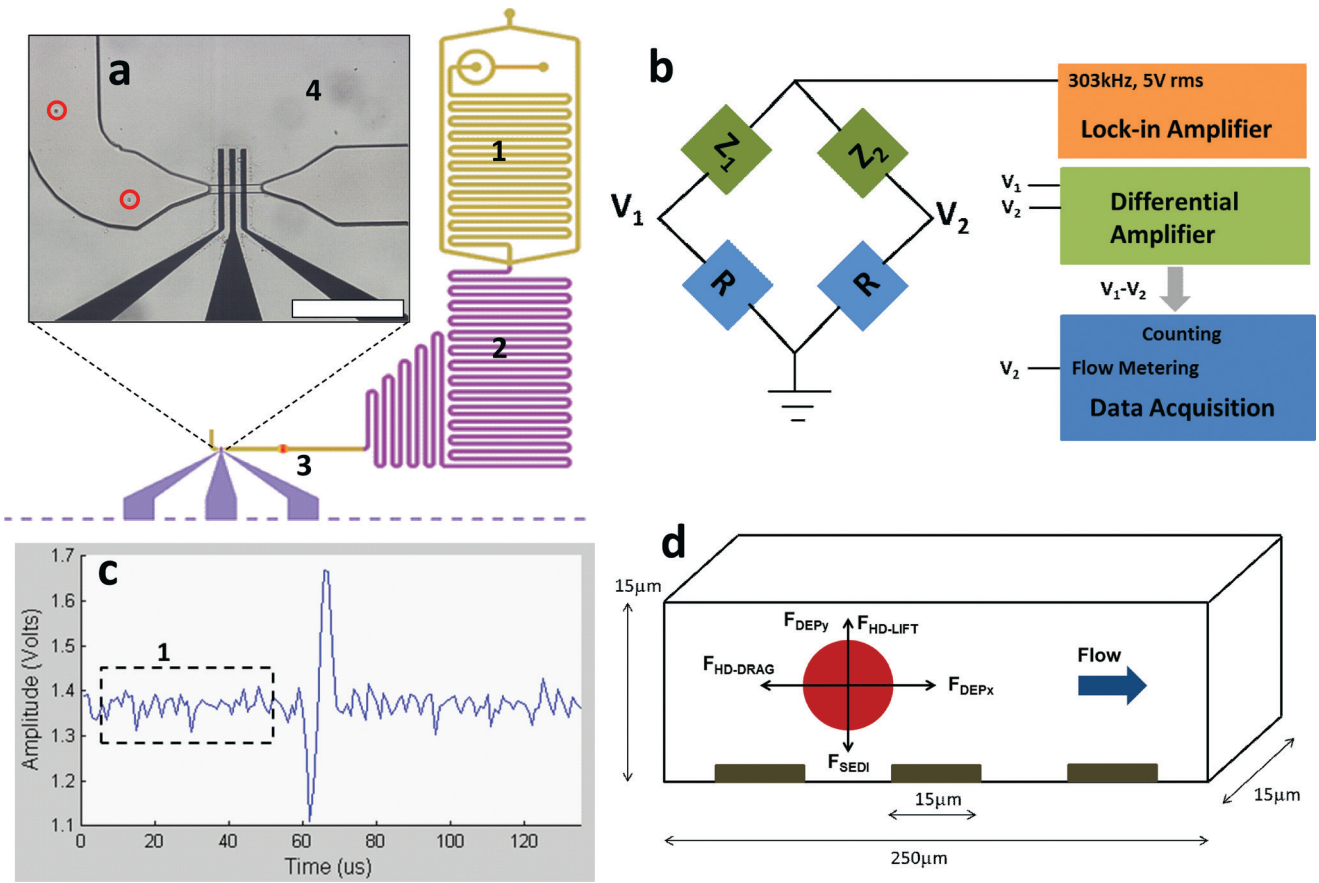

Fig. 1 Experimental setup. (a) The device layout with lysing and quenching modules are shown. 1. The lysing region, where erythrocytes get lysed. 2. The quenching region to preserve the leukocytes. 3. The cell counting/metering region with a 15 μm × 15 μm cross-section with electrodes. 4. Enlarged segment of (3); the red circles show the typical leukocytes passing through the measurement channel.[17] (b) The electrical measurement setup for cell counting and flow metering. The lock-in-amplifier (LIA) is used to inject the 303 kHz signal to the electrodes. The signal is acquired using a Wheatstone bridge. Metering is done by measuring the potential drop across R. However, for cell counting the differential signal is used. (c) A typical bipolar voltage pulse obtained as a result of the differential signal. The dotted rectangle, labeled as 1, is used to calculate the mean value of the baseline shift for the flow metering measurement. (d) The cross-section of the measurement channel depicting all the hydrodynamic and electrical forces exerted on the cells as they pass through the measurement channel.

the pH and osmolarity of the solution and thus preserving the remaining leukocytes.[18] The lysed blood solution passes through the measurement channel with a cross-section of 15 μm × 15 μm with micro-fabricated electrodes used for both cell counting and flow metering. Fig. 1a also shows the electrodes with the measurement (counting/metering) channel and the leukocytes (encircled in red) passing through the channel. The electronic measurement setup for flow characterization is shown in Fig. 1b. Z_1 and Z_2 represent the impedance in between the middle and the side electrodes and R is the 10 kΩ resistance connected as part of the Wheatstone bridge circuit. The input signal of 5 V at 303 kHz is fed to the middle electrode. Two different referenced signals are collected, first, a differential V_1–V_2 signal for cell counting using a differential amplifier, and second, a V_1 or V_2 voltage signal that is ground referenced. Fig. 1c shows the differential signal, which is a bipolar pulse for each passage of a cell across the electrodes. The height of the pulse depends on the size of the cell and the distance above the electrodes, whereas the pulse width depends on the flow rate. As we show later, the baseline of the signal also depends on the flow rate of the solution and its average value can be used to meter the flow rate.

A cell while flowing through the measurement channel experiences mechanical and electrical forces as shown in Fig. 1d. The sedimentation force, hydrodynamic drag force, hydrodynamic lift force and dielectrophoresis force are exerted on the cell and can alter its trajectory, thus resulting in a change of the electrical signal obtained.

Results

Modeling and simulations

The simple equivalent electrical model of a cell passing through a microfluidic channel over the electrodes is given in Fig. 2a. A cell is shown as a circle with radius R_c and membrane capacitance C_m. The resistance of the solution consisting of the cell lysate, and lysing and quenching reagents is represented as R_{sol}. A and B are the platinum electrodes to which the electrical signal is applied. C_{dl} is the double layer capacitance formed at the interface of the fluid and the electrodes. The equivalent impedance model is given in Fig. 2b where the model elements have been replaced by their equivalent impedance parts. The equivalent impedance between the electrodes is given in Fig. 2c. The change in impedance between the electrodes depends on the position of the cell from the electrodes, generating a higher impedance when the cell is near the electrodes. The same microfluidic channel including the electrodes and a biological cell flowing through it, was also simulated in COMSOL 4.2b. Fig. 2d shows the cross-sectional view of the channel and surface plot of the electrical field lines when a cell is placed near the top of the channel. Fig. S2† shows the corresponding electric potential surface plot. The change in impedance can be measured as the change in output voltage and thus can be used to characterize the cell's position, cell's velocity, and the fluid flow rate. Fig. 2e shows the increase in impedance as the cell approaches the electrodes at the bottom of the channel.

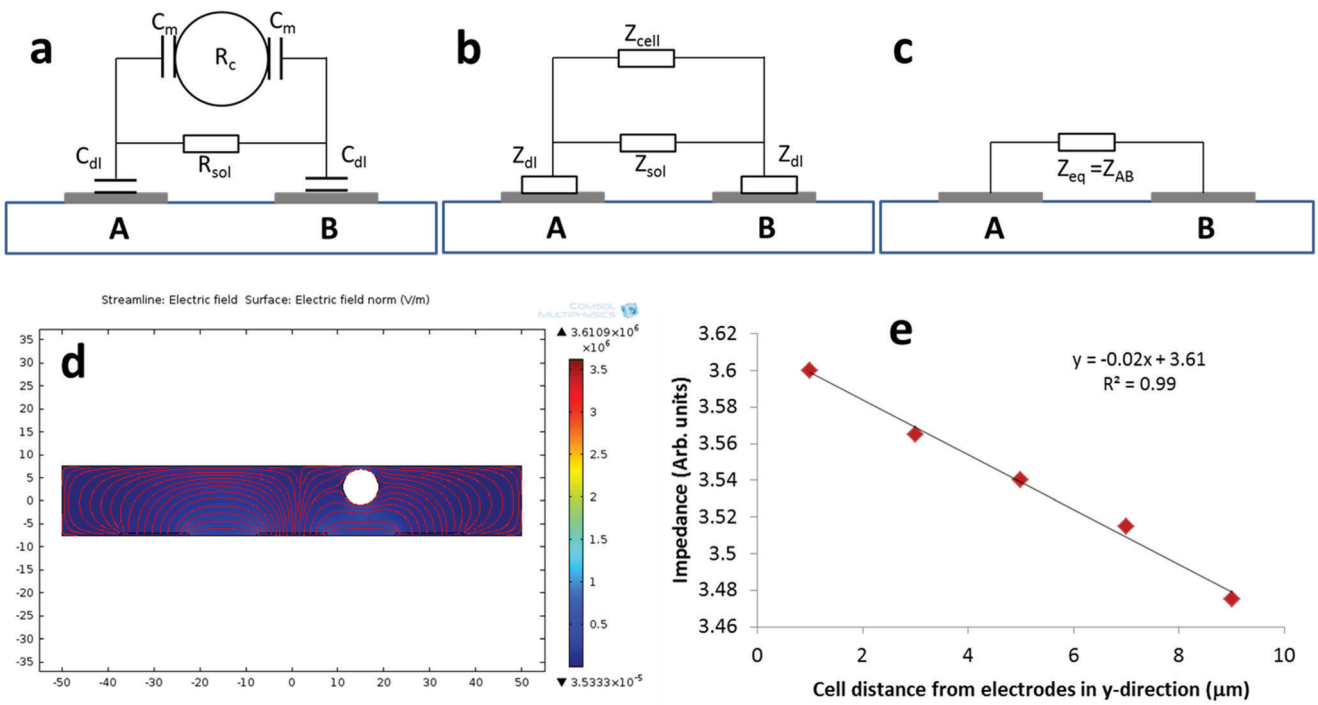

Fig. 2 (a) Equivalent electrical model of the cell and electrodes in the counting channel. (b) The corresponding impedance model of the circuit given in a. (c) The equivalent simplified impedance model of the circuit represented in b. (d) The simulation in COMSOL shows the normalized electrical field lines when the cell is near the top of the channel. (e) The impedance between electrodes decreases as the distance of the cell increases from the bottom of the channel.

Flow characterization with signal baseline shift

The amplitude change in the baseline of the voltage signal acquired is used for the flow metering as shown in Fig. 3. The flow rate varies from 10 μL min^{-1} to 60 μL min^{-1}, with an increment of 5 μL min^{-1}, and while keeping the flow rate constant for about 120 seconds the change in the baseline amplitude of the ground referenced signal is measured. First, the voltage change in the baseline is measured while flowing the lysing and quenching solutions together, which linearly increases with the increase in flow rate with an R^2 value of 0.99 as shown by the blue points in Fig. 3a. The blood is then infused with the lysing and quenching reagents and the change in the baseline shift is recorded with varying flow rates. These results also show a highly linear correlation (R^2 = 0.99) with a slightly lower amplitude than when using only lysing and quenching solutions. To investigate the variability in the baseline shift, we tried 3 different blood samples with different hematocrit values of 43.9, 46.5, and 39.8, and found that there is a very small change in slope of the linear regression line of the baseline signal amplitude *vs.* flow rate, *i.e.* 2.50, 2.52, and 2.36, respectively, as shown in Fig. S1.† It should be noted that the flow can also be metered by measuring the change in the baseline shift of the differential signal V_1–V_2, which also increases linearly with increasing flow rate with a high correlation (R^2 = 0.97) as shown in Fig. 3b.

Electrical cell counting for cell flux characterization

After the lysing of the erythrocytes, the remaining leukocytes pass through the electrodes and generate a bipolar pulse during their passage. The bipolar pulse obtained from the differential signal V_1–V_2 can also be used for cell counting, with each bipolar pulse representing a cell. The height of the pulse depends on the cell size and distance above the electrodes, with smaller cells generating smaller amplitude pulses. Fig. 4a shows a bipolar pulse generated for a typical lymphocyte (with an average radius of 3.9 μm). However, Fig. 4b shows a higher amplitude bipolar pulse generated for granulocytes or monocytes, which have a larger size with an average radius of 4.7 μm. The histogram in Fig. 4c represents the pulse count at different pulse amplitudes and shows the two distinct distributions for lymphocyte and granulocyte/monocyte populations. The number of the cells can be counted by either selecting the positive or the negative pulse. The threshold value *Th.*, as shown in Fig. 4c with the black arrow, is the voltage amplitude value used for cell counting. The threshold value is selected by considering the minimum voltage amplitude between the lymphocyte distribution and debris. Fig. 4c shows the histogram obtained for the negative pulse. The positive pulse is of higher magnitude as compared to the negative pulse, and the difference can be observed in Fig. 4(a and b). This difference is also clear from the shift in the histogram as indicated by the arrows i and ii, which represent the peak amplitude values for lymphocyte and granulocyte/monocyte distributions, respectively. The peak amplitude values of i and ii obtained for the negative pulse are 0.3 and 0.7 volts, and for the positive pulse are 0.45 and 0.95 volts, respectively. This difference in amplitudes should be considered while selecting the threshold value for cell counting either from the positive or the negative pulse.

Flow characterization with cell counting (cell flux)

With an increase in flow rate, the number of cells flowing through a measurement channel per unit time would also increase. Fig. 5a shows the linear relationship between the increase of cells flowing per minute and the increase in flow rate with a high correlation of (R^2 = 0.97). However, the number of cells present in one microliter of solution would remain constant when the flow rate increases. In experiments with varying flow rates, the number of cells μL^{-1} passing through a cross-sectional area of electrodes in one minute is calculated and shown in Fig. 5b. The average number of cells μL^{-1} in one minute, measured with varying flow rates of 10–60 μL min^{-1},

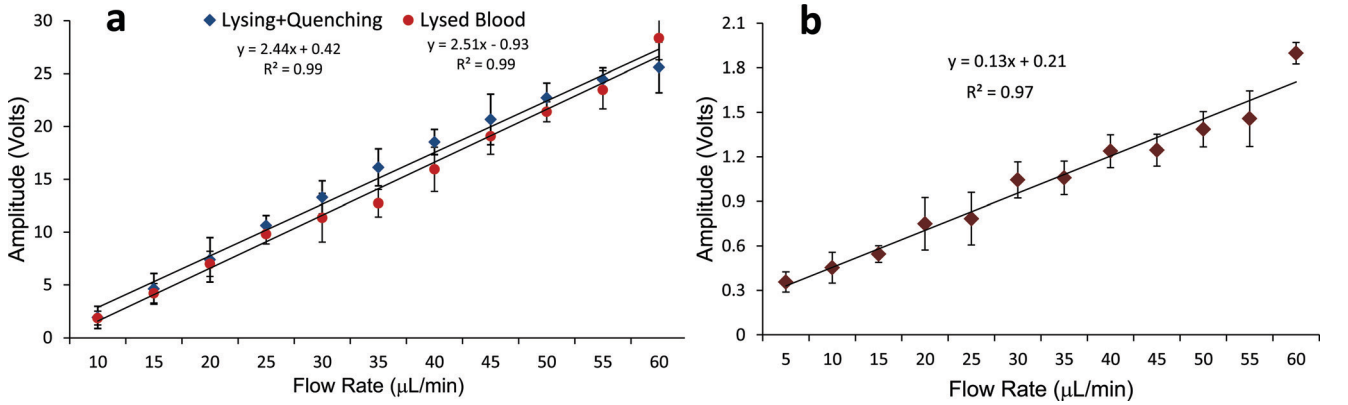

Fig. 3 Flow metering of the lysed blood in the measurement channel. (a) The linear relationship between the amplitude increase of the baseline signal (*i.e.* V_2 or V_1 ground referenced signal measured) and the increase in flow rate with lysing + quenching solutions (R^2 = 0.99) and lysed blood (R^2 = 0.99). The change in amplitude with a varying flow rate between lysed blood and lysing + quenching solutions does not show much difference. (b) The linear relationship between the increase in baseline signal (*i.e.* V_1–V_2, the differential voltage signal) and the increase in flow rate (R^2 = 0.97). Error bars represent one standard deviation across 3 experiments.

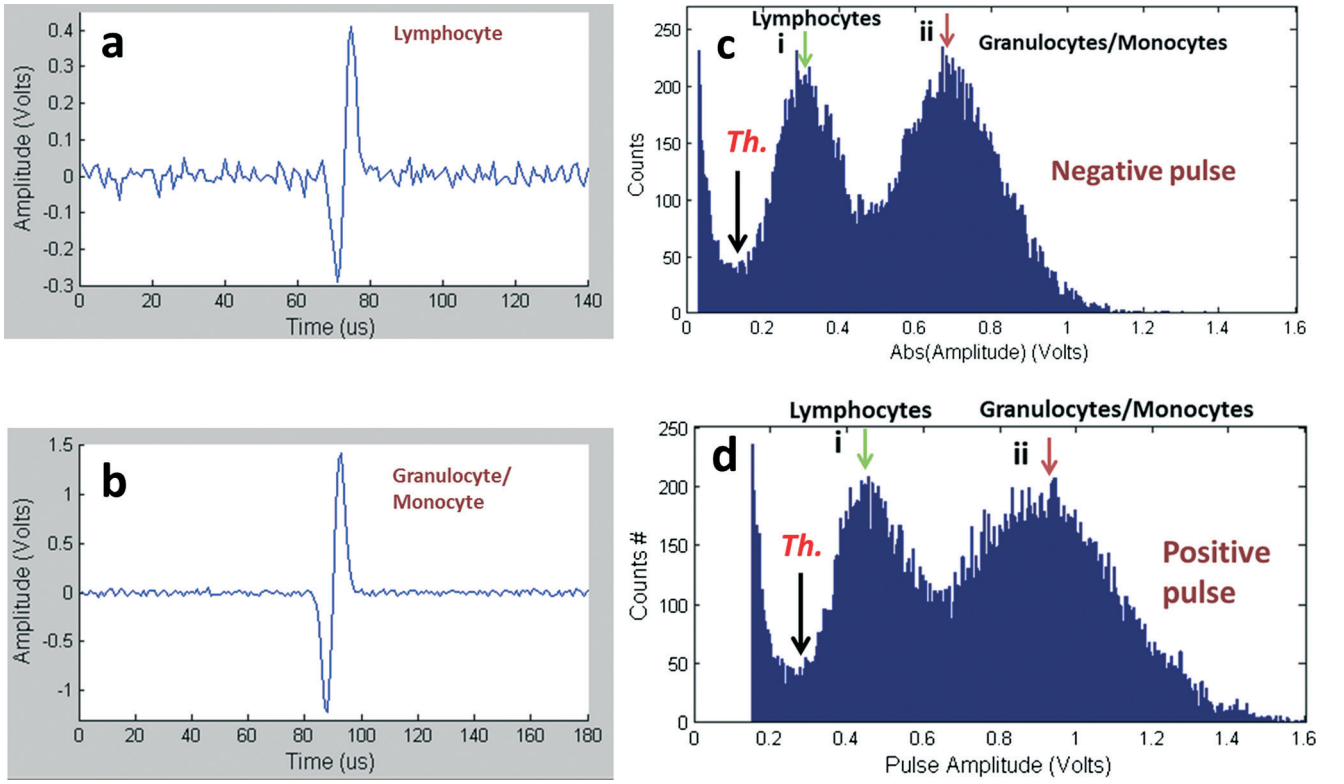

Fig. 4 The threshold selection for the cell counting method. (a) A typical bipolar pulse for a lymphocyte. (b) A typical bipolar pulse for a granulocyte/monocyte. As it is clear from these bipolar pulses, the positive pulse is of higher magnitude than the negative pulse, showing that the cell moves downwards as it moves along the measurement channel. (c) The histogram shows the two distributions of lymphocytes and granulocytes/monocytes by analyzing the negative pulse. (d) The histogram shows the two distributions of lymphocytes and granulocytes/monocytes by analyzing the positive pulse. *Th.* is the threshold voltage amplitude used for cell counting. The voltage shift in amplitude is about 0.2 volts. The peak amplitudes of the lymphocyte and granulocyte/monocyte distributions, represented as i and ii, for the negative pulse are 0.3 and 0.7 volts and for the positive pulse are 0.45 and 0.95 volts, respectively.

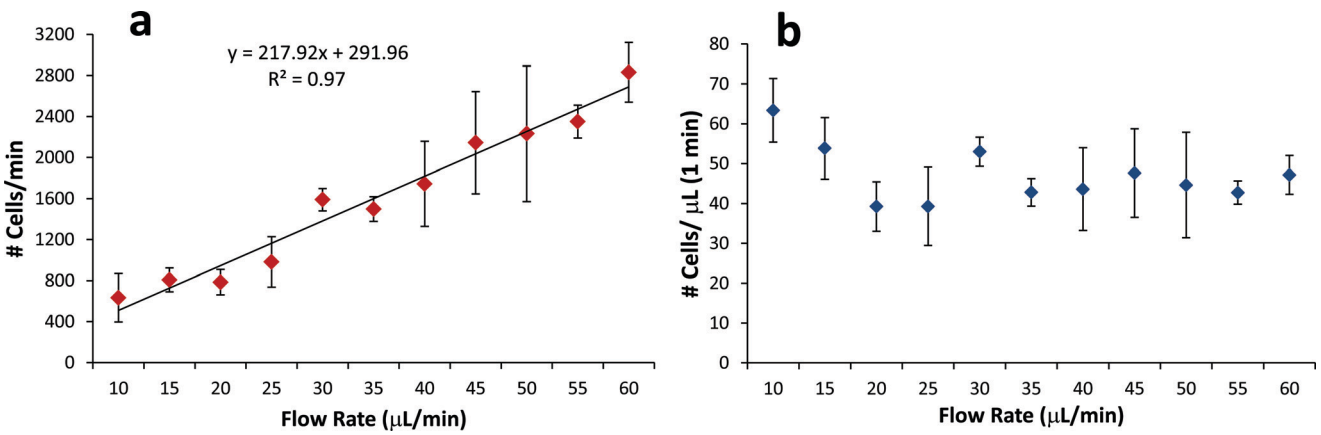

Fig. 5 (a) A linear relationship exists between the flow rate and the number of cells passing through the channel per unit time with a high correlation of (R^2 = 0.97). (b) The number of cells μL^{-1} is the ratio of cells min^{-1} : flow rate. This ratio should be constant with varying flow rates. For the 10–60 $\mu L\ min^{-1}$ range, the average value of cells μL^{-1} in one minute is 47 with one std. = 7 cells μL^{-1}. The accuracy is 5.42%. Error bars represent one standard deviation across 3 experiments.

is found to be 47 with a std. of 7 cells μL^{-1}. The number of cells μL^{-1} in a unit time should remain constant. However there is a variation in the number of cells μL^{-1} with increasing flow rate as shown in Fig. 5b. This can be attributed to a cell counting error within that one minute time period, which could be reduced by computing the number of cells μL^{-1} for higher time intervals. The difference between the cells μL^{-1} and the mean value of cells μL^{-1} (47 cells μL^{-1}) over the entire flow rate range *vs.* the flow rate is plotted in Fig S3.† This plot shows the variation of the data and 95% limits of agreement.

Flow metering with a change in pulse width

The width of the pulses generated as the cell passes through the electrodes depends on how fast the cell is flowing. We found that the pulse width is inversely proportional to the flow rate, thus, the mean value of the pulse width can also be used to determine the flow rate. Fig. 6 shows the relationship between the monotonic decrease in pulse width as the flow rate increases from 10–60 μL min^{-1}, with a correlation of R^2 = 0.87. The mean value of the pulse width, once pre-calibrated, can also be used to characterize or determine the flow rate of the fluid in which the cells were suspended.

Characterization of the pulse height

We found that the positive pulse is of higher amplitude than its negative pair, as shown in Fig. 4. Fig. S4† shows the plots of the mean amplitude for the positive pulse, the negative pulse, and mean of the difference between their amplitudes. The mean amplitude of the positive pulse is always higher than that of the negative pulse at all flow rates. Fig. S4a† shows the relationship between the mean pulse amplitude and increasing flow rate for lymphocytes. Fig. S4b† shows the relationship between the mean pulse amplitude and increasing flow rate for the granulocyte/monocyte population.

Discussion

The flow rate characterization of our approach is based on cell counting applications which usually require a flow rate to be around 10–100 μL min^{-1}. The dynamic range of the flow rate in our experiments is 10–60 μL min^{-1}. As compared to our approach, the optical fiber cantilever based flow characterization[1] gives an ultra-wide dynamic range of 10–1500 μL min^{-1}, where the minimum detectable change in the flow rate is about 31 μL min^{-1} for DI water.

The increase in impedance with the flow rate depends on the ionic concentration of the solution. For different blood samples, the number of erythrocytes varies from 3.26 to 5.99 million cells per microliter of blood (mean = 4.7 million cells, standard deviation = 0.46 million cells). This difference in number results in different ionic concentrations of the fluids after the erythrocyte lysis, thus resulting in different slopes for the linear relationship of the increase in impedance with the increase in flow rate as shown in Fig. S1.† The slope increases when the hematocrit value of the blood sample increases. The baseline amplitude difference corresponding to the different slopes is less for the lower range of the flow rates. However, if we compute the flow rates from equations given in Fig. S1† for the amplitude values from 5 to 30 V, the coefficient of variance (CV) value decreases from 0.12 to 0.05, while the standard deviation increases from 0.27 to 0.59. The reason for the decrease in the CV value is because the rate of the change of the standard deviation is much smaller as compared to the rate of the change of the flow rate. In the current experiments, with a dynamic range of 10–60 μL min^{-1}, the current calibration curve for flow metering would work for all blood samples. However a new calibration curve will be needed if the fluid sample is flowing at much higher flow rates or if different concentrations of the lysing and quenching buffers are used.

The flow metering based on the change of baseline amplitude shows a high correlation when compared to the characterization with pulse width and cell flux. Furthermore, the change in the baseline shift of the ground referenced signal is much higher (20 times) as compared to the change of the baseline amplitude of the differential signal. However, the main advantage of determining the flow rate by the pulse

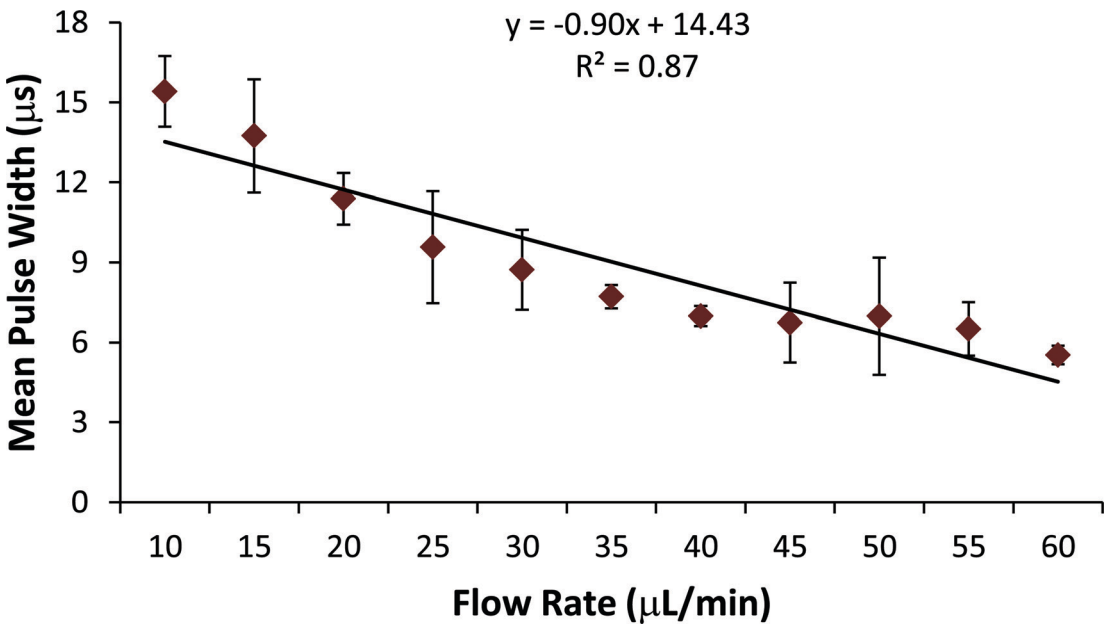

Fig. 6 The linear relationship between the pulse width and varying flow rate. The pulse width can also be calibrated and used for flow metering. Error bars represent one standard deviation across 3 experiments.

width is that it is independent of the small changes in the ionic concentration that may arise due to the difference in red blood cell concentration in the blood samples. However, the flow metering based on the cell flux is more sensitive to the variation of the number of blood cells in different samples. The strength of the proposed approach is that by acquiring a single voltage differential signal, the baseline amplitude, cell flux and pulse width, all can be measured. Thus, using a single signal, the flow rate characterization can be done by all techniques.

The accuracy in estimating the flow rate with the number of cells passing through the counting channel per unit time depends on the cell density in the solution. In healthy individuals, there are on average about 6000 leukocytes μL^{-1} with a standard deviation of 500–800 cells μL^{-1}. This variation in density of cells in a sample could be a source of error. For every 5 $\mu L\ min^{-1}$ change in flow rate, the mean change of cell flux is about 220 cells min^{-1}, as shown in Fig. 5a. A 10% variation in the blood cell count would produce a change of around 30 cells. This would limit the flow rate detection to approximately 2 $\mu L\ min^{-1}$. However, for all clinical blood cell counting applications there will be much more variation in the cell concentration range. Furthermore, for simultaneously performing cell counting and flow metering characterization, the cell flux approach cannot be applied directly. In such applications, the volume will be metered by the baseline shift or pulse width method and the cell concentration will be computed, which can be further used to meter the volume.

The amplitude impedance change between the positive and negative pulse could have resulted due to the application of hydrodynamic forces on the cells as they pass through the measurement channel, thus changing the relative position of the cell to the electrodes. The high flow rates 20–60 $\mu L\ min^{-1}$ would result in a significant drag force greater than the sedimentation and the lift force (ESI†).[19,20] However, it should also be noted that the fabrication inaccuracies between the three electrodes, due to the small variation in the platinum deposition and the electronics, might also be the source of error for the variation in the impedance amplitude of the pulses. Another possibility is the increase in hydrophobicity of the polydimethylsiloxane (PDMS) devices over time. Oxygen plasma treatment of PDMS results in producing reactive silanol groups on the surface which reorient back to the bulk over time during "hydrophobic recovery". An increase in hydrophobicity also increases the fluid contact angle on the PDMS surface, which might create more resistance to the fluid flow and could be a source of error of amplitude variation in the pulse. The measurement of this amplitude change is important while selecting the threshold value for the positive or negative pulse for accurate cell counting and in turn flow characterization through cell flux.

Conclusions

In this paper, a microfluidic cell counter is characterized for electrically metering the sample volume using the same electrodes that are used to count the cells. We demonstrate that there is a linear increase in the signal impedance as the flow rate is increased. We also show that the volumetric flow rate can be characterized electrically and that the pulse width decreases and cell counts per unit time increases with the increase in flow rate. These approaches can be very useful in measuring the sample volume in electrically based cell counting devices.

Materials and methods

Chip fabrication

The platinum electrodes were patterned on a Pyrex glass substrate by evaporating a 25 nm Ti adhesion layer and 75 nm Pt conduction layer and then lifting off undesired metal using standard photolithographic metal lift off procedures. Microfluidic channels were created by patterning a SU-8 thick negative photoresist (Microchem) as a negative master in which polydimethylsiloxane (PDMS) was poured and cured. Fluidic inlets and outlets were cored into the cured PDMS chips before permanently bonding them to the glass/electrode layer using oxygen plasma bonding.

Blood sample collection

The blood samples used in the study were collected from University of Illinois student volunteers through proper Institutional Review Board (IRB) approval. Blood was drawn *via* venipuncture into EDTA-coated BD Vacutainers (BD Biosciences). After the blood draw, the blood was kept on a sample rotisserie at room temperature until used for the experiments on the same day.

Modelling equations

Equations in Fig. 3, 5, and 6 do not represent a physical relationship between the flow rate and voltage amplitude, pulse width or cell flux. The equations are not dimensionally consistent as well. These equations represent the modelling equations to characterize the flow rate from voltage amplitude, pulse width or cell flux.

Acknowledgements

The authors would like to acknowledge the help of G. Damhorst for drawing the blood from healthy student donors. Funding: R. Bashir acknowledges the support of the NSF NSEC at OSU grant number EEC-0914790, National Science Foundation Industry-University Collaborative Research Center for Agricultural, Biomedical, and Pharmaceutical Nanotechnology at the University of Illinois at Urbana-Champaign, and funding from the University of Illinois, Urbana-Champaign.

References

1 V. Lien and F. Vollmer, *Lab Chip*, 2007, 7, 1352.

2 H. Ernst, A. Jachimowicz and G. Urban, *Sens. Actuators, A*, 2002, **100**, 54.
3 T. Nakagama, T. Maeda, K. Uchiyama and T. Hobo, *Analyst*, 2003, **128**, 543.
4 R. Kliese, Y. Lim, E. Stefan, J. Perchoux, S. Wilson and A. Rakić, *Conference on Optoelectronic and Microelectronic Materials and Devices (COMMAD)*, Canberra, Australia, 2010, pp. 7–8.
5 H. Yu, D. Li, K. Xu, R. Roberts and N. Tien, *Conference on the Advances in Optoelectronics and Micro/Nano-Optics (AOM)*, Guangzhou, China, 2010, pp. 1–5.
6 H. Ayliffe and R. Rabbitt, *Meas. Sci. Technol.*, 2003, **14**, 1321.
7 R. F. Probstein, *Physicochemical Hydrodynamics*, John Wiley & Sons, Inc., Hoboken, 2nd edn, 2003.
8 B. J. Kirby and E. F. Hasselbrink Jr., *Electrophoresis*, 2004, **25**, 187.
9 P. D. I. Fletcher, S. J. Haswell and X. Zhang, *Lab Chip*, 2001, **1**(2), 115.
10 J. A. Cooper and R. G. Compton, *Electroanalysis*, 1998, **10**, 141.
11 K. Y. Tam, J. P. Larsen, B. A. Coles and R. G. Compton, *J. Electroanal. Chem.*, 1996, **407**, 23.
12 A. C. Fisher, *Electrode Dynamics*, Oxford Chemistry Primers, Oxford University Press, Oxford, 1996.
13 J. Collins and A. Lee, *Lab Chip*, 2004, **4**, 7.
14 V. G. Levich, *Physicochemical Hydrodynamics*, Prentice Hall, Englewood Cliffs, NJ, 1962.
15 I. Moser, G. Jobst and G. Urban, Laboratory on chip for clinical applications, in *Micro-total Analysis Systems*, Kluwer Academic Publishers, Dordrecht, 1998.
16 E. H. Ernst, A. Jachimowicz and G. Urban, *Proceedings of the Conference Eurosensors XIV*, Copenhagen, Denmark, 2000.
17 N. N. Watkins, U. Hassan, G. Damhorst, H. Ni, A. Vaid, W. Rodriguez and R. Bashir, *Sci. Transl. Med.*, 2013, **5**, 214ra170.
18 N. N. Watkins, S. Sridhar, X. Cheng, G. D. Chen, M. Toner, W. Rodriguez and R. Bashir, *Lab Chip*, 2011, **11**, 1437.
19 H. Li and R. Bashir, *Biomed. Microdevices*, 2004, **6**, 289.
20 H. Li, Y. Zheng, D. Akin and R. Bashir, *Journal of Microelectromechanical Systems*, 2005, **14**, 103–112.

